THE TREND IN ASYMMETRIC DRIFT ACROSS THE BLUE CLOUD

KYLE B. WESTFALL[1], MATTHEW A. BERSHADY[2], KEVIN BUNDY[1], ET AL.

Draft: 14 Feb 2017

ABSTRACT

Using the statistical prowess of the SDSS-IV/MaNGA survey, we demonstrate a strong trend between the strength of lag of the stellar rotation curve behind that of the ionized gas as a function of its absolute luminosity.

Keywords: galaxies: kinematics and dynamics — galaxies: spiral — galaxies: structure

1. MOTIVATION

Asymmetric drift is the lag of the ensemble stellar rotation speed behind the circular speed defined by the gravitational potential. For stellar ensembles, Binney & Tremaine (2008, Section 4.4.3) provide an intuitive description of asymmetric drift as arising due to the combined effect of the radially decreasing surface-density and velocity-dispersion profiles typical of axisymmetric systems. Using the v_R moment of the collisionless Boltzmann equation, one obtains the Jeans (ref) equation that directly relates the circular speed (v_c), the mean stellar tangential speed ($\overline{v_\theta}$), and the stellar velocity ellipsoid (SVE) as a function of radius in the plane of symmetry:

$$v_c^2 - \overline{v_\theta}^2 = \sigma_R^2 \left[\frac{\sigma_\theta^2}{\sigma_R^2} - \frac{R}{\rho\sigma_R^2} \frac{\partial(\rho\sigma_R^2)}{\partial R} - 1 \right] - R\frac{\partial\overline{v_R v_z}}{\partial z}, \quad (1)$$

where R, θ, z are the cylindrical coordinates, ρ is the volume density, and σ is the velocity dispersion. Along with the standard assumptions of dynamical equilibrium and negligible radial and vertical flows inherent to its derivation, equation 1 is often simplified by assuming the rightmost term — describing the covariance between the radial and vertical motions as a function of perpendicular distance to the plane of symmetry — is negligible (cf. Cuddeford & Amendt).

Asymmetric drift has been measured in numerous systems. Perhaps most notably, e.g., Dehnen & Binney have shown that populations of stars show a direct correlation between their velocity dispersion and the degree to which their mean rotation speed lags behind that of the Local Standard of Rest (LSR), much in line with the expectation provided by equation 1. Although there have been some studies of asymmetric drift in external galaxies (refs), it is often treated as a nuisance phenomenon that must be corrected for when trying to constrain the circular speed curve of a galaxy (refs). The ubiquity and phenomenology of asymmetric drift as a salient observable has not yet been studied for a statistically significant population of galaxies. Our aim is therefore to provide a first look at the correlation between asymmetric drift measurements and basic broad-band photometric properties for a large sample of galaxies.

Electronic address: westfall@ucolick.org

[1] UCO/Lick Observatory, University of California, Santa Cruz, 1156 High St., Santa Cruz, CA 95064, USA

[2] Department of Astronomy, University of Wisconsin-Madison, 475 N. Charter St., Madison, WI 53706, USA

In addition to the basic understanding of this dynamically relevant quantity, our interest in asymmetric drift stems from its fundamental dynamical connection to the full phase-space distribution function of a galaxy's stars, as empirically demonstrated in the Milky Way. Indeed, Westfall et al. (2011) (see also refs) used asymmetric drift to constrain the axial ratios of the SVE given direct measurements of the line-of-sight (LOS) stellar velocity dispersion, σ. Alternatively, if one can statistically constrain the shape of the SVE (refs), measurements of asymmetric drift could be used as a proxy for stellar σ by either appealing to equation 1 or an empirical relation calibrated by samples with both asymmetric drift and σ measurements. Such a use of asymmetric drift as a proxy for stellar σ is attractive in the low-surface-brightness and low-velocity-dispersion regimes where direct measurements are difficult and/or expensive. We commit to this paradigm by using the following nomenclature for asymmetric drift, following from equation 1:

$$\sigma_a^2 \equiv v_c^2 - \overline{v_\theta}^2. \quad (2)$$

For disk galaxies, there is a decades-long industry of using cold-gas tracers to construct circular-speed curves of galaxies (refs). These data have provided the first concrete arguments for the presence of massive dark-matter halos (ref) based on mass model reconstruction (refs) and have formed the basis for the most robust Tully-Fisher relations compiled for the local Universe (refs). However, it is important to acknowledge that one cannot directly measure v_c, effectively making σ_a unobservable. That is, every dynamical tracer has some non-zero dynamical pressure such that it will lag behind the theoretically defined circular speed. There are very clear examples of early-type galaxies that show differential asymmetric-drift in their molecular (e.g., CO), atomic (e.g., H I), and/or ionized (Hα) tracers relative to a robust mass model of v_c (Davis et al.) due to the different turbulent/thermal pressures intrinsic to these tracers. However, these signatures are much less apparent in disk galaxies. For example, Martinsson et al. show that Hα and H I rotation curves are consistent for the DiskMass Survey within the limits of their constraints on beam-smearing, suggesting that any correction for the lag of either behind the circular speed should be small. Indeed, theoretical calculations (Dalcanton & Stilp) suggest that gas-pressure corrections to H I rotation curves should be largely negligible for galaxies with $\mathcal{M} > 10^x \mathcal{M}_\odot$. Nevertheless, we emphasize here that our measurements of
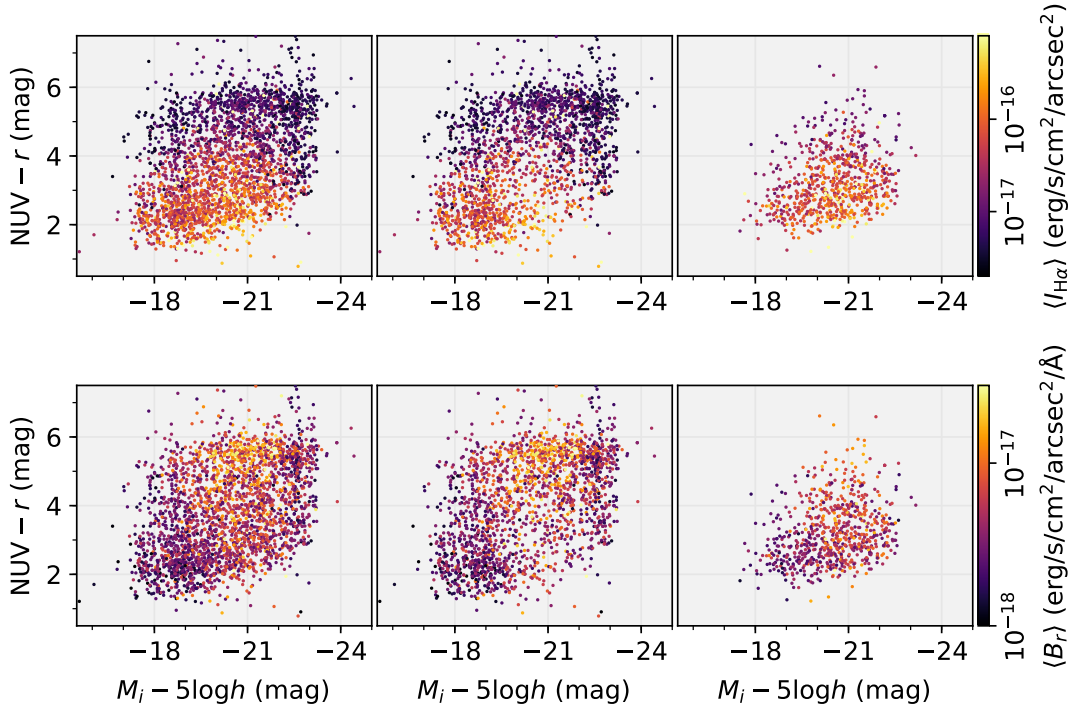
Figure 1. N$-r$ color and absolute i-band magnitude (M_i) for all galaxies observed during the first two years of the MaNGA Survey (left), the subsample of galaxies *not* selected to be kinematically regular (middle; see text), and the asymmetric-drift sample used throughout the remainder of our analysis. The color of the data points in the top row represent the mean Hα surface brightness [[check aperture]] according to the colorbar to the right; the bottom row replaces the color by the r-band surface brightness density.

σ_a may be better termed as a *differential tangential lag* because they are based on the quadrature difference between the observed Hα and stellar rotation curves in our galaxy sample (Section 2). These measurements are perfectly valid in their own right; however, it is their interpretation in the context of the theoretical definition of asymmetric drift that should be questioned in some regimes, as discussed in Section 4.

We present the data used for our analysis in the following section. In Section 3, we demonstrate that there is a strong correlation between the absolute i-band magnitude of a galaxies and the strength of its asymmetric drift measured at half of an effective radius (0.5 $R_{\rm eff}$). We also illustrate the weak color dependence in this relation. We summarize and discuss these results in Section 4.

2. DATA

We use integral-field spectroscopy from the SDSS-IV/MaNGA (Mapping Nearby Galaxies from APO) Survey to construct stellar and ionized-gas velocity fields for 2715 unique galaxies, 39 of which have multiple observations. The kinematic measurements are provided by the MaNGA data analysis pipeline (DAP; Westfall et al., in prep): the ionized-gas kinematics are based on simple single-Gaussian fits to the Hα emission feature and the stellar kinematics are determined using pPXF (Cappellari et al.) with the MILES stellar template library (Jesus FB et al.).

The MaNGA galaxy selection (Wake et al. in prep) is a simple cut in absolute i-band magnitude, M_i, and redshift, z, and provides a complete sampling of the overall galaxy population. As such, measurements of stellar

and/or Hα rotation curves for some systems will be difficult/impossible. Using the photometry from the NASA-Sloan Atlas (ref),[3] Figure 1 shows the color-magnitude diagram of all galaxies colored by their mean Hα and r-band surface brightness. [[TODO: Need to check this plot.]] Although not excluded from our velocity-field analysis *a priori*, we expect to obtain poor rotation curve measurements for galaxies with low Hα and stellar surface brightness.[4]

[[Extinction corrections for the CMD?]]

We model the geometric projection of the rotational plane of each galaxy using the approach presented by Andersen & Bershady (2013); see also Westfall et al. (2011). In three independent fitting iterations, the model fits are optimized for the Hα velocity field, the stellar velocity field, and simultaneously for both data sets; for the latter, the geometry is forced to be the same for the two dynamical tracers, but the parametrized rotation curves are independent. We use these velocity-field-fitting results to objectively isolate a set of "kinematically regular" galaxies. Briefly, galaxies in this sample must have: (i) successful velocity-field fits for all three approaches, (ii) differences in the measured Hα and stellar systemic velocity of less than 20 km s^{-1}, (iii) dynamical centers that are consistent to within a fiber diameter of the morphological center [[check]], (iv) Hα and stellar velocity-field position angles that are consistent to within $\pm15°$, and (v) kinematic inclinations between $15° < i < 80°$

---

[3] nsatlas.org

[4] The uniformity of the MaNGA survey (Law et al. 2015) is such that S/N is tightly correlated with surface brightness.

that are both consistent between the Hα and stellar data and with respect to the photometric ellipticity to within $\pm 20°$. The constraint on the inclination is by far the most stringent. [[give number of galaxies cut by each criterion?]] Applying these constraints yields a sample of 798 observations (for 790 unique galaxies) out of the 2764 observations analyzed. Eleven galaxies with repeat observations satisfy the selection criteria; however, only five of these show all observations are consistently selected, whereas the other six show one or more of the observations did not pass our constraints [[we should understand this.]]. [[TBD: Finally, we also visually inspected the broad-band imaging of these 790 galaxies and eliminated merging and highly extincted (highly inclined) systems yielding a final sample of XXX galaxies.]] We hereafter refer to galaxies that satisfy our selection criteria as the "asymmetric-drift" sample.

Figure 1 shows the color-magnitude distribution for all MaNGA galaxies, as well as the distributions of those galaxies included and excluded from our asymmetric-drift sample. As expected, galaxies with relatively high Hα and r-band surface brightness are preferentially selected, excluding much of the red sequence as well as the brightest and faintest galaxies in the blue cloud. Although the conclusions we reach based on our asymmetric drift sample are astrophysically meaningful, it is important to appreciate the biased representation of the overall galaxy population represented by the sample in our analysis. [[Show histogram of kinematically regular sample against the volume-corrected distribution of the MaNGA parent sample in Mi and N-r, and discuss.]]

Our velocity-fitting method provides a model rotation curve fit to both the Hα and stellar data, each parametrized as a hyperbolic tangent function: $v_{\rm rot} = v_{\rm flat} \tanh(R/h_v)$. However, our primary result is based on the error-weighted mean of the deprojected rotation curve measurements for each dynamical tracer within $\pm 30°$ of the major axis and $2\farcs5$ radial bins centered at 0.25, 0.5, 0.75, 1.0, and 1.25 $R_{\rm eff}$ — $R_{\rm eff}$ is the effective radius using the elliptical Petrosian analysis from the NASA-Sloan Atlas. [[Check that $R_{\rm eff}$ includes the multiplicative offset to match these Petrosian and Sersic $R_{\rm eff}$ in the mean.]] Specifically, we calculate the error-weighted mean and standard deviation of $v_j = V_j / \cos\theta_j / \sin i$ and

$$\sigma_{a,j}^2 = (V_{{\rm H}\alpha,j}^2 - V_{*,j}^2)(\cos\theta_j \sin i)^{-2}, \qquad (3)$$

where V_j is the LOS measurement of each component in spaxel j located at the in-plane polar coordinates R_j and θ_j and i is the disk inclination.

[[An example demonstrating the details of our measurements is illustrated in Figure X.]]

We calculate errors in $v_{{\rm H}\alpha}$ and σ_a as the quadrature sum of the error-weighted standard error (i.e., the error-weighted standard deviation divided by $\sqrt{N}$) and the propagated error in the error-weighted mean. [[Can revisit this. Details of error calculation not all that important. We're dominated by intrinsic deviations from the regression.]]

3. RESULTS

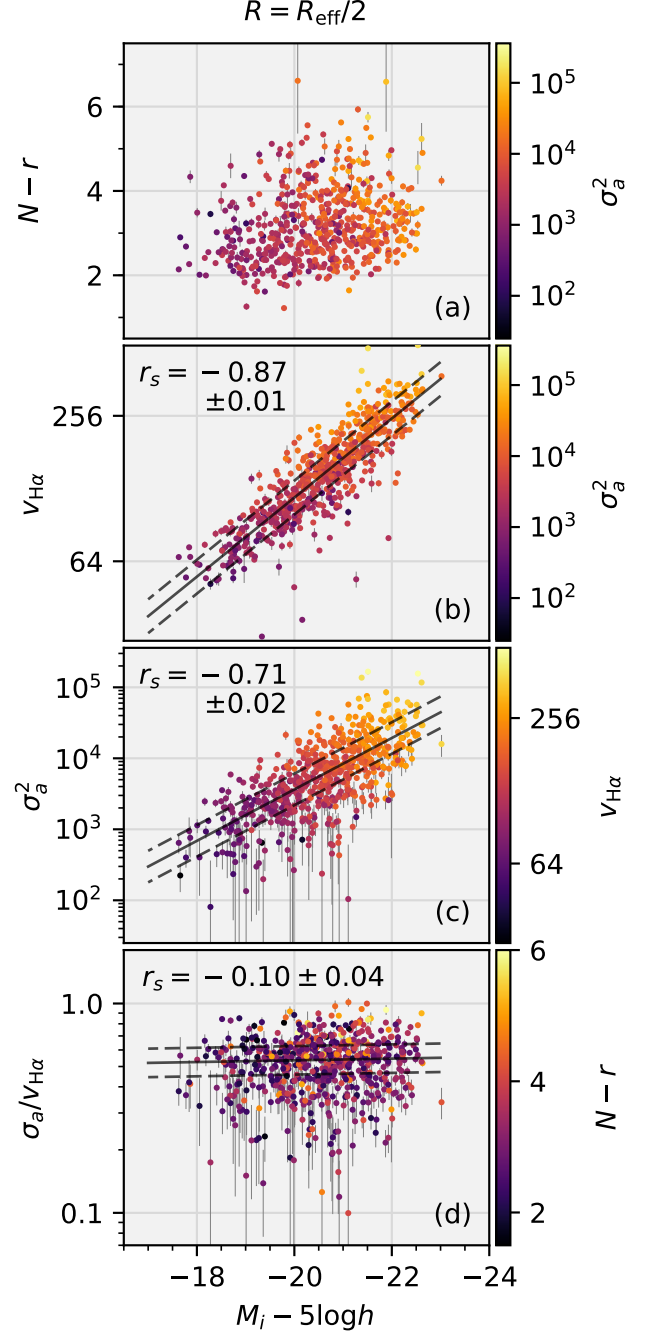Figure 2(a) shows the $(M_i, N - r)$ color-magnitude diagram (see right column of Figure 1) with the points

Figure 2. Global photometry measurements versus kinematics measurements at $R = R_{\rm eff}$ for the asymmetric-drift sample: M_i versus (a) $N - r$ color with each point colored according to σ_a^2, (b) $v_{{\rm H}\alpha}$ with each point colored according to σ_a^2, (c) σ_a^2 with each point colored according to $v_{{\rm H}\alpha}$, and (d) $\sigma_a/v_{{\rm H}\alpha}$ with each point colored by the $N - r$ color. Panels (b), (c), and (d) include the Spearman rank correlation coefficient, r_s, and the linear regressions (solid lines) constructed from the median parameters provided in Table 1. The dashed lines are offset from linear regression by the modeled intrinsic scatter in the relation (ε_y).

Table 1
Linear Regressions for M_i [[Check slope-intercept form]]

Parameter	Dependent Variable		
	$v_{\mathrm{H}\alpha}$	$\log(\sigma_a^2)$	$\log(\sigma_a/v_{\mathrm{H}\alpha})$
y_0	2.168 ±0.003	3.78 ±0.01	-0.269 ±0.003
ϕ	170.70 ±0.15	160.1 ±0.5	-0.24 ±0.17
ε	0.069 ±0.001	0.209 ±0.005	0.068 ±0.002
m	-0.164 ±0.003	-0.362 ±0.009	-0.004 ±0.003
b	-1.20 ±0.05	-3.69 ±0.19	-0.36 ±0.06
ε_y	0.070 ±0.001	0.222 ±0.005	0.068 ±0.002

colored according to σ_a measured at $R = 0.5R_{\mathrm{eff}}$. There is a clear trend where brighter galaxies have larger σ_a; the remainder of the Figure examines this trend.

We plot M_i versus $v_{\mathrm{H}\alpha}$, σ_a^2, and $\sigma_a/v_{\mathrm{H}\alpha}$ in Figures 2(b), 2(c), and 2(d), respectively. The points are colored according to the color bar and quantity to the right of each panel. Each panel provides the Spearman rank correlation coefficient, r_s, of the plotted data with errors derived from 10^3 bootstrap simulations. We have also used a Markov Chain Monte Carlo (refs) to sample the Bayesian posterior distribution for a linear regression to the data in each panel, incorporating the errors in both axes (refs); the errors in the kinematic quantities are always dominant. The fitted model is a line in parametric form with an intrinsic Gaussian scatter perpendicular to the line. That is, the line is defined as $\mathbf{l}(t) = \mathbf{l}_0 + t\,\hat{\mathbf{l}}$ for a generalized coordinate t along the line, an origin $\mathbf{l}_0 = \{x_0, y_0\}$, and the unit vector $\hat{\mathbf{l}} = \{\cos\phi, \sin\phi\}$. The fitted parameters are y_0, ϕ, and the dispersion of the intrinsic Gaussian scatter about the line, ε; x_0 is fixed at the median abscissa of the data being fitted ($x_0 = M_{i,0} = -20.6$). Uniform priors are used for y_0 and ϕ and a logarithmic prior [[check]] is used for ε (ref). Using the returned samples of the posterior, we also provide parameters for the slope-intercept form of the line — $y = mx + b$ where $m = \tan\phi$ and $b = y_0 - x_0\tan\phi$ — and the scatter projected along the ordinate, $\varepsilon_y = \varepsilon/|\cos\phi|$. Table 1 provides the median and standard deviation of the marginalized distribution of each parameter; these parameters have been used to construct the lines provided in Figure 2.

As expected, there is a strong correlation between $v_{\mathrm{H}\alpha}$ and M_i. However, it is important to note that Figure 2(b) does not present the Tully-Fisher (ref) relation for our asymmetric-drift sample; the Figure gives the rotation speed at $R = 0.5R_{\mathrm{eff}}$, not a measure of the full-width of the dynamically broadened line profile. The slope of the relation in Figure 2(b) is steeper than a nominal Tully-Fisher relation because galaxies at low luminosity tend to have more slowly rising rotation curves (refs), which can be confirmed by plotting $h_{v,\mathrm{H}\alpha}/R_{\mathrm{eff}}$ as a function of M_i. [[actually show this?]]

Figure 2(c) gives the direct representation of the gradient in the point color seen in Figure 2(a). The data in
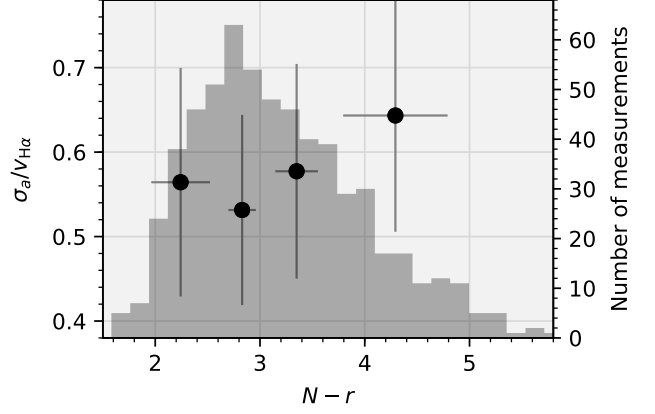

Figure 3. The error-weighted mean trend in $\sigma_a/v_{\mathrm{H}\alpha}$ binned in quartiles of the global $N - r$ color (black points). The error bars represent the error-weighted standard deviation of the data within each bin; the error-weighted standard error is smaller than the size of each black point. The underlying gray histogram provides the number of measurements in bins of $N - r$; each quartile contains ~152 galaxies.

this panel are highly correlated, both as determined by r_s and the fitted regression. The intrinsic scatter increases from 0.07 dex (17%) in $(M_i, v_{\mathrm{H}\alpha})$ to 0.21 dex (62%) in (M_i, σ_a^2); however, this is close to the ~0.1 dex scatter if considering (M_i, σ_a) instead.

If σ_a or $v_{\mathrm{H}\alpha}$ was a secondary parameter in the distribution of $(M_i, v_{\mathrm{H}\alpha})$ or (M_i, σ_a^2), respectively, we should expect a gradient in the point color in Figures 2(b) and 2(c) *perpendicular* to the fitted regression. However, we see that the primary gradient in point color is parallel to the fitted regression. This is consistent with the result that there is little to no correlation between M_i and $\sigma_a/v_{\mathrm{H}\alpha}$, as shown in Figure 2(d): Both r_s and ϕ are small and only marginally significant with respect to their errors. From equation 3, this implies that the deprojected stellar rotation is a roughly constant fraction of the ionized-gas rotation speed, with $v_* \sim 0.9v_{\mathrm{H}\alpha}$. Although the radius at which the asymmetric drift was sampled is different, this ratio is consistent with galaxies from the DiskMass survey (Martinsson et al.).

The points in Figure 2(d) are colored by the global $N - r$ color; however, it is difficult to determine from this illustration if their is any correlation between $\sigma_a/v_{\mathrm{H}\alpha}$ and global galaxy color. One might expect such a correlation if, for example, galaxies with different global color different light-weightings of the thin vs. thick-disk (refs [[not sure there are relevant ones]]), which propagates to a different dominant dynamical pressure in the disk mid-plane. Figure 3 assess this directly by plotting the error-weighted mean trend in $\sigma_a/v_{\mathrm{H}\alpha}$ for the quartiles of the $N - r$ distribution of the asymmetric-drift sample. The error bars represent the error-weighted standard deviation of the data in each bin, whereas the error-weighted standard error is always smaller than the plotted point. There is a marginal detection of a slightly larger $\sigma_a/v_{\mathrm{H}\alpha}$ in the reddest bin; however, more data would be required to lend this result any statistical significance.

4. DISCUSSION

4.1. *Technical Concerns*

[[Sample bias]]
[[Beam-smearing]]

4.2. *Prospects*

If σ_a is a direct proxy for σ_R ...

REFERENCES

Binney, J., & Tremaine, S. 2008, Galactic Dynamics: Second Edition (Princeton University Press, Princeton, NJ USA)